

Controlling Film Instabilities

E. Schäffer*, S. Walheim** and U. Steiner

Department of Polymer Chemistry and Materials Science Center, University of Groningen, NL-9741 AG Groningen, The Netherlands

*present address: Max Planck Institute of Molecular Cell Biology and Genetics, Pfotenhauerstrasse 108, D-01307 Dresden, Germany

**present address: Institut für Nanotechnologie, Forschungszentrum Karlsruhe, Postfach 3640, D-76021 Karlsruhe, Germany

Abstract

This conference contribution gives an overview of various aspects of instabilities in thin layers. Film instabilities are presented from two different viewpoints. Fundamentally, the study of instabilities allows to deduct interfacial interactions with great sensitivity. While from a technological angle film instabilities are usually undesired, we demonstrate two examples where film instabilities can be harnessed to create structures on length scales down to 100 nm.

1 Introduction

Technological applications usually require thin films, layers and coatings to be highly homogeneous. This requirement is dictated by the function of the layers. Coatings not only protect surfaces, modify their mechanical, rheological and corrosion behavior, but also fulfill an important function in design and fashion. In particular the latter function imposes conditions on the film homogeneity that are often difficult to meet. The colors of thin optical coatings, for example, are a function of the film thickness. Since the human eye is able to detect interference color changes that stem from film thickness changes as little as 1-2 nm, the quality of optical layers has to be controlled on this length scale.

Instabilities in thin films, while technologically undesired are interesting from a fundamental point of view. The break-up of thin films sensitively mirrors the minute forces that act at the film interfaces. The most extensively studied example of the effect of interfacial forces on film stability is the dewetting of thin supported polymer films [1,2]. In these studies, film instabilities occurred either spontaneously, driven by van der Waals forces [3], or was heterogeneously nucleated [4]. While this research on film dewetting

has elucidated the mechanisms that lead to film instabilities and has provided a theoretical framework, which is now commonly used to predict film stability [1,5], the control of film stability by tuning the van der Waals forces is difficult to achieve. In this overview of our research, we give two examples, how interfacial interactions that lead to a laterally heterogeneous film formation can be used to control the structure formation process in thin films.

The ability to precisely control film instabilities is not only useful for detailed fundamental studies. The modification of the lateral morphology in thin films opens up new possibilities for several practical applications. Examples of this are a new way to manufacture anti-reflective coatings [6] or novel lithographic techniques [7,8].

In the following sections, we describe two different mechanisms for the controlled creation of laterally heterogeneous films: polymer-polymer demixing [9] and electrohydrodynamic instabilities [10]. In addition, possible applications of these techniques are discussed [6-8].

2 Polymer-Polymer Demixing in Thin Films

Most binary polymer couples are immiscible. This is both experimentally as well as technologically an inconvenience. Practically all studies on the phase behavior of binary polymer melts were carried out on the relatively rare weakly incompatible polymer pairs.

2.1 Phase Morphology of Supported Films

Here, we have studied the demixing of strongly incompatible blends during spin-coating, as schematically illustrated in Fig. 1a [9]. Polystyrene (PS, molecular weight $M_w = 95$ kg/mol) and polyvinylpyridine (PVP $M_w = 115$ kg/mol) were dissolved in tetrahydrofuran (THF) (1.5 weight percent) and a film was prepared by spin-coating. During the film formation process, THF evaporates and once the polymer concentration reaches ~10%, PS-PVP phase separation sets in. Since the two polymers have different surface- and interfacial tensions with respect to the air and substrate surface, the substrate is expected to play a dominant role in the phase separation process. In Fig. 1b,c, atomic force microscopy (AFM) images of the PS-PVP phase morphology after spin-coating are shown. PS/PVP films deposited onto a polar gold surface exhibit a bilayer morphology. The more polar PVP completely wets the gold substrate and is in turn wetted by the less polar PS, which minimizes the surface tension of the film sandwich (Fig. 1b,c top). In regions, where the

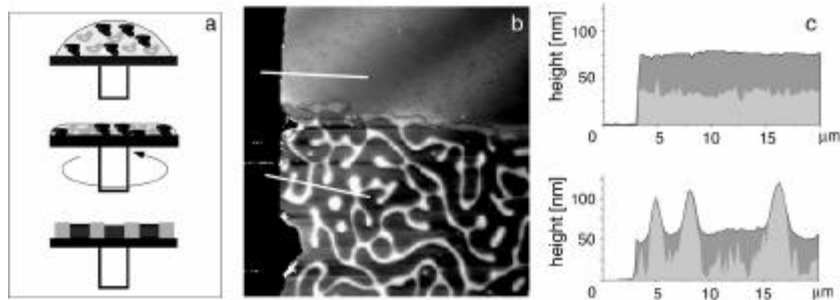


Figure 1 : (a) Schematic representation of polymer-polymer demixing upon spin-coating. (b) AFM image of a PS/PVP mixture after spin-coating onto gold (upper half) and a non-polar surface (lower half). (c) The corresponding cross-sectional polymer compositions (white lines in (b)).

gold surface was rendered non-polar with the help of a self assembled monolayer, the specific segregation of PVP and PS to the substrate is reduced and both phases partially wet the substrate, leading to the lateral phase morphology in Fig. 1b,c bottom.

2.2 Lithography by Demixing

The principle introduced in the previous section can be employed as a lithographic technique [7]. The principle is schematically shown in Fig. 2. We start with a structured silicon master pattern, which was obtained by electron-beam lithography. Onto this topographic surface, a polydimethyl-siloxane precursor was cast and chemically cross-linked to form a rubber stamp. In a second step, the surface of the rubber stamp was soaked in an octadecyl mercaptan solution and placed onto a gold covered silicon wafer. In places where the rubber touched the gold, a densely packed hydrocarbon self-assembled monolayer formed. This technique, known as micro-contact printing (μ CP) [11] creates a lateral variation in surface energy on the substrate, with a negligible variation in topography. Subsequently, a PS/PVP/THF mixture was spin-cast onto the patterned surface. The structured polymer film that was created this way can then be further processed. For example, one of the polymers can be removed using a selective solvent (e.g. cyclohexane to remove PS or ethanol to remove PVP). This way, a lithographic polymer mask featuring a relatively high aspect ratio is made.

Experimental results of this lithographic technique are shown in Fig. 3. The upper left part of Fig. 3a shows, how the PS-PVP phase separation is influ-

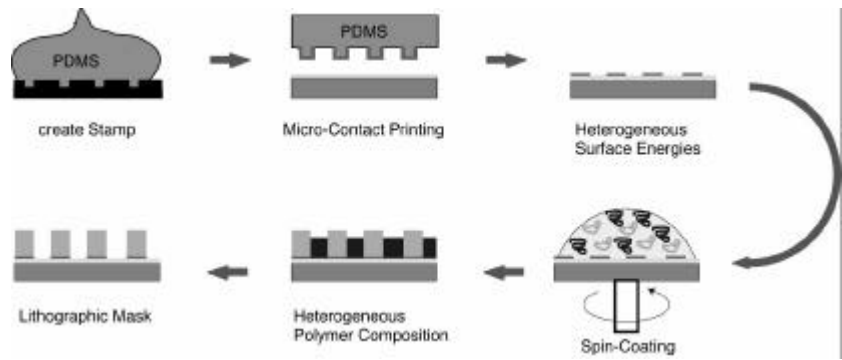


Figure 2: Schematic representation of the lithography by demixing.

First, a rubber stamp is cast from a master. By μ CP, a patterned self-assembled monolayer is stamped onto a gold surface and a PS/PVP mixture is spin-cast onto the patterned surface. Subsequently one of the polymers (e.g. PVP) is removed by a selective solvent

enced by a line pattern (2.4 μ m periodicity) made by μ CP. The lower right part of Fig. 3a was not pre-patterned by μ CP and the PS-PVP phase morphology similar to Fig. 1b (bottom) is recovered. Fig. 3b shows a three dimensional representation of an AFM scan of the PS lines after removal of the PVP phase. The remaining PS stripes mirror the pattern that was imposed by μ CP. The rectangular cross-section of the PS stripes is an essential feature of this technique. As opposed to ridges with spherical cross-sections that characterize the partial wetting of a liquid on a surface, the straight side walls and sharp edges of the polystyrene stripes (described in detail in [9]) are an important prerequisite of a lithographic structure.

2.3 Anti-Reflective Coatings

While a detailed control of the lateral structure is required for the lithography application in the previous section, it is sometimes sufficient to merely fine-tune the length scale that characterizes the polymer-polymer phase morphology. This is shown in Fig. 4. By changing (1) the molecular interactions of the two polymers used, and (2) their molecular weights, it is possible to vary the characteristic size and spacing of the phase-separated domains by several orders of magnitude. Particularly interesting is the case in Fig. 4b, where both length scales are on the order of 100 nm, smaller than the wavelength of visible light. Similar to the previous experiment, it is possible to remove one of the two polymer phases with a selective solvent, creating a porous film.

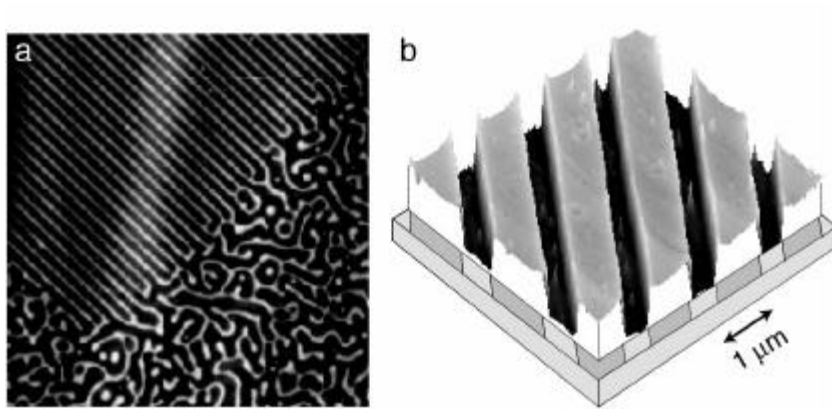


Figure 3: (a) PS/PVP mixture spin cast onto a stripe patterned gold surface. (b) A three dimensional representation of the PS stripes after the PVP was selectively removed

Macroscopically, the film in Fig. 4a appears opaque due to the scattering of light at the domain boundaries. The more finely structured film in Fig. 4b, on the other hand, is completely transparent since the light “averages” over the pores and the remaining polymer material. Such films have a refractive index that is determined by the volume fraction of air in the film.

The control over the film’s refractive index makes such layers suitable as antireflective (AR) coatings [6]. To fully suppress the reflection of light (at perpendicular incidence), AR coatings have to fulfill two requirements: (1) the light reflected from the air-film and film-substrate surface has to be phase shifted by $\lambda/2$. For a film of refractive index n_f , this implies that the film thickness must be $1 / 4n_f$; (2) complete destructive interference requires the

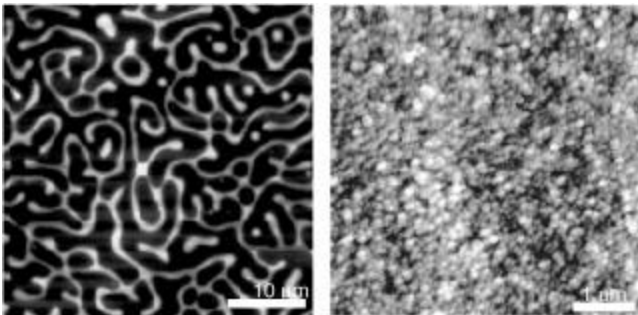


Figure 4: AFM images of (a) a spin-cast PS-PVP film (both ~ 100 kg/mol) and (b) a PS/PMMA film (both ~ 10 kg/mol).

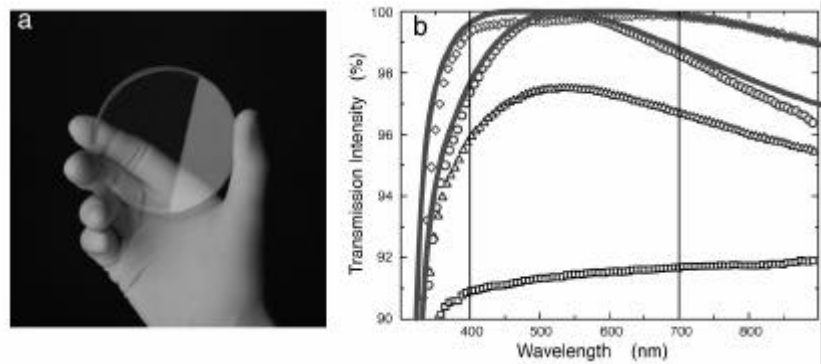


Figure 5: (a) Plexiglas disk coated on both sides with porous polymer antireflection coatings (partially removed on the right hand side). (b) Optical transmission through a microscopy slide: squares: uncoated; triangles: MgF_2 coating $n_f = 1.38$; circles: nanoporous PMMA coating $n_f = 1.23$; diamonds: double layer coating. The calculated lines are theoretically optimal one and two layer coatings.

partially reflected amplitudes to be equal. This defines a condition for the refractive index of the film: $n_f = \sqrt{n_0 n_s}$, where n_0 and n_s are the refractive indices of air and the optical substrate, respectively. While conventional coatings can easily satisfy the first condition, the second requirement is more difficult to meet. For an air-glass interface, for example, we have $n_0 = 1$ and $n_s = 1.5$, and therefore $n_f = 1.22$. Since the lowest refractive indices of solid-state materials are ~ 1.3 , heterogeneous layers are required.

In Fig. 5a, a Plexiglas disk was on both sides covered with nanoporous PMMA layers. On the right-hand part of the disk, the layers were removed to display the contrast between AR coated and untreated surface areas. Fig. 5b shows transmission spectra of uncoated and coated microscopy slides. As opposed to conventional coatings, nanoporous coatings increase the optical transmission to almost 100% at the wavelength of the transmission maximum. A double-layer coating reduces the rest reflection of the slide to less than 0.5% averaged over the entire visible spectrum.

While there are various ways to introduce porosity or roughness on a 100 nm scale (in fact, Fraunhofer's original discovery of the AR effect was based on this principle), the length scale selectivity is an important characteristic of our technique. Simply etching the surface, for example, introduces roughness on all length scales. This results in a reduction in specular reflection, but intro-

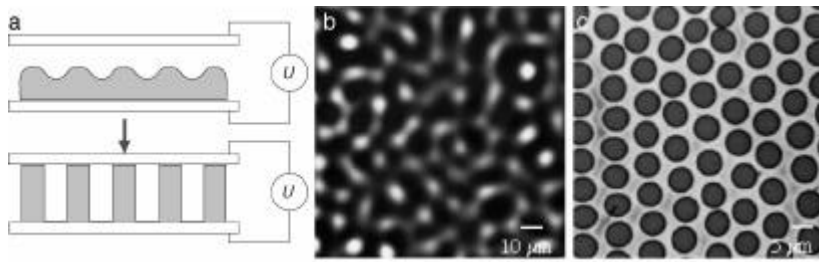


Figure 6: (a) Experimental setup for the electrostatic structure formation experiment. (b) Early and (c) late stage of the electrohydrodynamic instability

duces scattering of light from larger surface structures. As a result, the surface is “tarnished”. Very recently, we have improved the mechanical properties of the porous films by combining the demixing of macromolecules with a sol-gel step that produces a porous mineralized layer with good mechanical properties and good adhesion to glass and transparent plastics.

3 Structure Formation by Electric Fields

A further way to trigger film instabilities can be achieved by the interaction of an electric field with an interface between two media of different dielectric constants [10]. Qualitatively, different polarizabilities of the two materials result in a partial loss of displacement charge compensation at the interface, leading to the formation of a charge double-layer at the interface, if a component of the electric field lies perpendicular to the interface. If both dielectric materials are liquid, a configuration of lower free energy can be reached by aligning the interfaces parallel to the electric field. This effect is the cause of an electrostatic destabilizing force that acts at the interface.

3.1 Electrohydrodynamic Film Instabilities

The experimental setup is shown in Fig. 6a. A polymer film (e.g. PS, $M_w = 100$ kg/mol) was spin-cast onto a silicon wafer, which served as one of the electrodes. A second silicon wafer was mounted facing the polymer film, leaving an air gap, and a voltage (~ 50 V) was applied. In this configuration, an electrostatic force acts at the polymer-air surface, destabilizing the film [8]. After annealing above the glass transition of the polymer for a period of time, the assembly was cooled down to room temperature, the top wafer was removed, and the polymer film was investigated by optical microscopy and AFM. The initially flat polymer film developed first a surface undulation

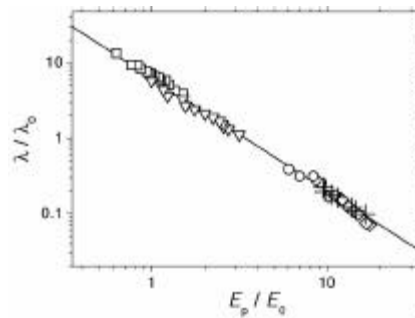


Figure 7: Instability wavelength λ (from images similar to Fig. 6b,c) as a function of the electric field in the polymer film E_p . Both, λ and E_p are plotted in reduced coordinates, in which all experimental parameters are scaled out [10]. The different symbols correspond to a wide variety of experimental parameters.

with a characteristic length scale, as shown in Fig. 6b. With time the surface waves were amplified until they touched the upper plate to form columns. The final configuration is shown in Fig. 6c: hexagonally arranged vertical columns. The lateral order stems from a repulsion of the wave maxima and minima in Fig. 6b, caused by differing interfacial polarization charges, which depend on the local film thickness [8].

Theoretically, the instability can be understood in the framework of a linear stability analysis [10]. In the absence of a destabilizing force (e.g. van der Waals force), surface tension stabilizes thin films. The action of an electric field, however, overcomes the stabilizing effect of the surface tension. The electrostatic pressure acting at the polymer–air interface can be obtained by writing down the energy stored in the capacitor and by taking the derivative with respect to the local vertical position of the interface (the only free variable parameter in the set-up). A linear stability analysis yields the unstable mode λ . Qualitatively, λ is determined by three factors: the surface tension, the film viscosity, and the electrostatic force. Very small values of λ require the creation of a large polymer-air surface area. This is unfavourable in terms of the surface free energy of the film. Very large values of λ , on the other hand, require the displacement of polymer over large lateral distances. While thermodynamically allowed, this requires a long time. Long wavelength instabilities are therefore pre-empted by instabilities with smaller wavelengths. The balance between these two factors results in the emergence of an instability with a very narrow distribution of λ values that is exponentially amplified.

Fig. 7 shows the comparison between the results of the linear stability analysis and the experimental results [10]. The relatively simple model describes the experimental data, in the absence of any fit parameters.

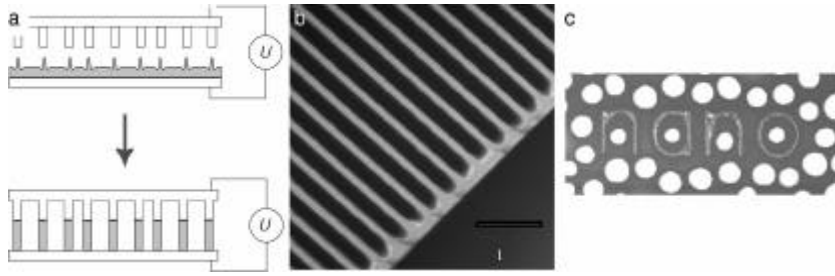


Figure 8: (a) Schematic setup of the electrohydrodynamic lithography experiment. (b) Replicated line pattern (line width = 100 nm). (c) Replication of the word “nano”.

3.2 Electrohydrodynamic Lithography

The principle outlined in the previous section can be harnessed as a lithographic technique [8]. To this end, one of the planar electrodes is replaced by a topographic master (Fig. 8a). In our experiments, we used the same patterned silicon wafer that was employed in the manufacture of stamps for micro-contact printing in section 2.2. In the case of a patterned top electrode in Fig. 8a, the electric field is laterally inhomogeneous. Since the destabilizing electrostatic force is a function of the electric field, the deformation of the polymer air surface is strongest at the locations, where the electrode topography extends downward towards the polymer film. The film is first destabilized at these locations and, with time, the polymer is drawn towards the direction of highest electric field gradient.

The result of this is shown in Fig 8b,c. The structured polymer film faithfully replicated the master electrode. Similar to the replication by demixing in section 2.2, the length scale of the structures on the master must approximately match λ . This requirement is not very strict in the case of the electrohydrodynamic replication technique, as shown in Fig. 8c. Here, the instability first replicated the master pattern (the word “nano”). After a much longer time, the remaining film became unstable, forming columns, which exhibited a much larger value of λ compared to the stroke width of the lines (300 nm). This also illustrates that the exposure time of the liquid film to the electric field is an important parameter in the replication process.

Note that this replication mechanism is fundamentally different compared to imprinting techniques, where the master is pressed into the liquefied polymer film at high pressures. During imprinting, all the air between the template and the film has to be removed, leading often to Hele-Shaw-type fingering instabilities of trapped air, disrupting the replications process. Also, the large

polymer-template contact area makes the release of the master tricky. In contrast, in our technique, the polymer is drawn up towards the master, preventing air-inclusion problems and simplifying mask release, due to the small contact area between the polymer and the master.

4 Conclusions

The exploitation of film instabilities to create, control and replicate patterns in polymer films is extremely versatile. The two techniques described above – polymer-polymer demixing in thin films and electrohydrodynamic film instabilities – are merely two examples of a more widely applicable principle. Almost any force that acts on a thin film or a surface can be exploited (i) as a measurement tool to study physical phenomena at surfaces and interfaces, and (ii) to create or replicate patterns for a variety of applications.

5 References

1. Brochard-Wyart, F. and Daillant, J. Drying of solids wetted by thin liquid films, *Canadian Journal of Physics*, **68**, 1084-1088 (1990)
2. Reiter, G Dewetting of thin polymer films, *Phys. Rev. Lett.* **68**, 75 (1992)
3. Seemann, R.; Herminghaus, S. Jacobs, K. Gaining control of pattern formation of dewetting liquid films, *J. Phys Cond. Mat.*, **13**, 4925 (2001)
4. Jacobs, K.; Mecke, K. and Herminghaus, S. Thin liquid polymer films rupture via defects, *Langmuir*, **14**, 965-969 (2001)
5. Vrij, A., Possible mechanism for the spontaneous rupture of thin, free liquid films, *Discussions of the Faraday Society*, **42**, 23-33 (1966)
6. Walheim, S.; Schäffer, E.; Mlynek, J. and Steiner, U. Nanophase-separated polymer films as high-performance antireflection coatings, *Science*, **283**, 520-522 (1999)
7. Böltau, M.; Walheim, S.; Mlynek, J.; Krausch, G. and Steiner, U. Surface-induced structure formation of polymer blends on patterned substrates, *Nature*, **391**, 877-879 (1998)
8. Schäffer, E.; Thurn-Albrecht, T.; Russell, T.P. Steiner, U. Electrically induced structure formation and pattern transfer, *Nature*, **403**, 874 (2000).
9. Walheim, S.; Böltau, M.; Mlynek, J.; Krausch, G. and Steiner, U. Structure Formation via Polymer Demixing in Spin-Cast Films, *Macromolecules*, **30**, 4995-5003 (1997)
10. Schäffer, E.; Thurn-Albrecht, T., Russell, T.P. Steiner, U. Electrohydrodynamic instabilities in polymer films, *Europhy. Lett.*, **53**, 518 (2001)

11. Xia, Y. and Whitesides, G. M., Soft Lithography, *Angewandte Chemie-International Edition*, **37**, 550-575 (1998)